Received: 12 May 2021 | Revised: 11 September 2021 | Accepted: 15 September 2021

DOI: 10.1096/fj.202100443R

THE FASEB JOURNAL

RESEARCH ARTICLE

Differential expression and hypoxia-mediated regulation of the N-myc downstream regulated gene family

Nguyet Le | **Timothy M. Hufford** | **Jong S. Park** | **Rachel M. Brewster**

Department of Biological Sciences, University of Maryland, Baltimore County, Baltimore, Maryland, USA

Correspondence
Rachel M. Brewster, Department of Biological Sciences, University of Maryland, Baltimore County, Baltimore, MD 21250, USA.
Email: brewster@umbc.edu

Funding information
HHS | NIH | National Institute of Child Health and Human Development (NICHD), Grant/Award Number: R21HD089476; HHS | NIH | National Institute of General Medical Sciences (NIGMS), Grant/Award Number: R25GM055036, T32 GM066706 and T34 HHS 00001; DOD | Center for Neuroscience and Regenerative Medicine (CNRM), Grant/Award Number: RT150086

Abstract

Many organisms rely on oxygen to generate cellular energy (adenosine triphosphate or ATP). During severe hypoxia, the production of ATP decreases, leading to cell damage or death. Conversely, excessive oxygen causes oxidative stress that is equally damaging to cells. To mitigate pathological outcomes, organisms have evolved mechanisms to adapt to fluctuations in oxygen levels. Zebrafish embryos are remarkably hypoxia-tolerant, surviving anoxia (zero oxygen) for hours in a hypometabolic, energy-conserving state. To begin to unravel underlying mechanisms, we analyze here the distribution of the N-myc Downstream Regulated Gene (*ndrg*) family, *ndrg1-4*, and their transcriptional response to hypoxia. These genes have been primarily studied in cancer cells and hence little is understood about their normal function and regulation. We show here using in situ hybridization that *ndrgs* are expressed in metabolically demanding organs of the zebrafish embryo, such as the brain, kidney, and heart. To investigate whether *ndrgs* are hypoxia-responsive, we exposed embryos to different durations and severity of hypoxia and analyzed transcript levels. We observed that *ndrgs* are differentially regulated by hypoxia and that *ndrg1a* has the most robust response, with a ninefold increase following prolonged anoxia. We further show that this treatment resulted in *de novo* expression of *ndrg1a* in tissues where the transcript is not observed under normoxic conditions and changes in Ndrg1a protein expression post-reoxygenation. These findings provide an entry point into understanding the role of this conserved gene family in the adaptation of normal cells to hypoxia and reoxygenation.

Abbreviations: AP-1/2, activator proteins 1 & 2; Cap43, calcium-associated protein 43 kDa; CREB, cAMP-response element binding protein; Drg1, downregulated gene 1; EPO, erythropoietin; HIF-1α, hypoxia-inducible factor 1 alpha; HRE, hypoxia response element; Igfbp-1, insulin-like growth factor-binding protein 1; LAMP1, lysosomal-associated membrane protein 1; Myc, myelocytomatosis proto-oncogene, basic helix-loop-helix transcription factor; NDRG, N-myc downstream regulated gene; NF-kB, nuclear factor kappa-light-chain-enhancer of activated B cells; PHD2, prolyl hydroxylase domain protein 2; PROXY-1, protein regulated by oxygen 1; Rab4, Ras-related protein Rab-4A; Rit42, reduced in tumor, 42 kDa; RTP, reducing agents and tunicamycin-responsive protein; STAT, signal transducer and activator of transcription; TNF-α, tumor necrosis factor alpha; VEGF, vascular endothelial growth factor; VHL, von Hippel-Lindau protein; WISH, wholemount in situ hybridization.

Nguyet Le and Timothy M. Hufford contributed equally to this study.

KEYWORDS
gene expression, hypometabolism, hypoxia, NDRG, zebrafish

1 | INTRODUCTION

Earth's atmosphere is composed of approximately 21% oxygen (O_2). Aerobic organisms use this environmental O_2 to produce ATP during oxidative phosphorylation. Hence, fluctuations in O_2 levels (either up or down) can have very detrimental outcomes for aerobic organisms. Severe hypoxia causes a decrease in ATP production due to diminished activity of the electron transport chain. Given that ATP fuels energy-demanding processes in the cell, its reduction can lead to cellular damage or death.[1–4] Thus, hypoxia, hypoxemia or ischemia, is a contributing cause to many disease states in humans, including pulmonary vascular disease, acute kidney injury, neurodegenerative disease, and stroke.[5–10] Conversely, excessive O_2 is equally, if not more harmful as it causes oxidative stress due to reactive oxygen species production that is damaging to macromolecules, including lipids, proteins, and nucleic acid.[11–13]

To mitigate these adverse consequences, aerobic organisms have evolved mechanisms to adapt to low O_2 and maintain homeostasis. Such adaptations optimize access to O_2 by increasing red blood cell count and angiogenesis and altering energy metabolism, in part by switching from oxidative phosphorylation to glycolysis.[14,15] In addition, cells conserve energy when exposed to chronic and severe hypoxia by reducing their metabolic rate. The latter is accomplished via suppression or arrest of energetically demanding processes such as cell division, transcription and translation, and down-regulating the activity of the sodium-potassium ATPase pump.[16–23] While metabolic suppression has primarily been studied in organisms considered anoxia-tolerant, including painted turtles, crucian carp, naked mole rats and hibernating ground squirrels,[16,24] it is likely to also be utilized in other organisms as well, albeit to a lesser extent. Zebrafish (*Danio rerio*) embryos maintain homeostasis under anoxia (zero O_2) by entering into a hypometabolic state characterized by reversible developmental and physiological arrest, which enables them to survive for up to 50 h.[25,26] This protective response is developmentally regulated, with older embryos being less tolerant to anoxia.[26]

Despite the necessity to conserve energy via suppression of transcription and translation, genes that are vital for the hypoxia response are in fact transcriptionally up-regulated under hypoxia.[27–30] Such up-regulation is mediated by several transcription factors, the best studied of which is the Hypoxia-Inducible Factor-1α (HIF-1α).[31–33] Under normoxic conditions (normoxia), the HIF-1α subunit is hydroxylated by prolyl hydroxylase domain protein 2 (PHD2), marking it for degradation by the von Hippel-Lindau protein (VHL). However, when O_2 levels are reduced, PHD2 activity is inhibited and stabilized HIF-1α binds to the HIF-1β subunit and translocates to the nucleus to regulate transcription. Upon entry into the nucleus, HIF-α/β heterodimers bind the hypoxia-response element (HRE). Even though this sequence is abundant in the genome, fewer than 1% of potential HRE sites are bound by the HIF complex under hypoxia, suggesting the existence of another layer of regulation.[34–37] HIFs directly activate genes that mediate metabolic reprogramming from oxidative phosphorylation to glycolysis[38,39] and genes that increase the available O_2 supply, such as *EPO*, *VEGF*, and its receptors.[40] Other HIF targets are implicated in autophagy, apoptosis, redox homeostasis, inflammation and immunity, stemness and self-renewal, metastasis and invasion.[35,39,41,42] In addition to HIFs, several other transcription factors are known to influence the hypoxia response, including CREB, Myc, NF-kB, and STATs, which engage in cross-regulatory interactions with HIFs.[32]

Members of the N-myc downstream regulated gene (NDRGs) family are also hypoxia-responsive. The mammalian family consists of four members, *NDRG1-4*, while the zebrafish genome with its third round of genome duplication, encodes 6 paralogues, *ndrg1a*, *1b*, *2*, *3a*, *3b*, and *4*.[43] NDRGs are highly conserved across metazoans and the sequence homology is in fact greater for specific members of the family across different species (>80%) than between NDRG family members of the same species, which share ~57%–65% amino acid identity.[44] NDRGs belong to the α/β-hydrolase family, however, they are thought to be enzymatically inactive, lacking a critical catalytic triad.[45] NDRG1 (formerly known as Drg1, Cap43, Rit42, RTP, and PROXY-1) contains three tandem repeats (GTRSRSHTSE) near its C-terminal and a phosphopantetheine sequence, which are two unique features that make it distinct from other NDRG family members. NDRG1 is thought to function as a tumor suppressor.[46] However, the absence of cancer resultant from germline mutations in humans[47] and targeted knockout in mice,[48] suggests that *NDRG1* may rather be involved in cancer progression (metastasis) rather than initiation.[49–54] Human NDRG1 interacts with numerous other proteins in human cancer and other cell lines, including actin, Clathrin, and associated proteins AP-1 and AP-2, Caveolin-1, Kinesin, LAMP1, Rab4, and 26S proteasome components,[49,51,55,56] consistent with a possible role in regulating vesicle trafficking.[56,57] *NDRG1* and *NDRG2* transcript levels increase under hypoxia, as these genes have HIF-1α binding sites (hypoxia-response elements or HREs) in their promoters.[58–61]

However, NDRG regulation under hypoxic conditions is complex and does not depend solely on HIF-1α, as several other transcription factors[62,63] and *NDRG1* long non-coding RNA itself[64,65] have also been implicated. *NDRG4* is transcriptionally up-regulated under hypoxia in cancer cells, however, in a TNF-α/NF-κB rather than a HIF-1α -dependent manner.[66] In contrast, NDRG3 is regulated post-translationally in hypoxic cancer cells, via lactate binding, which stabilizes the protein and promotes cell proliferation and angiogenesis.[67] These findings indicate that NDRGs are regulated at the transcriptional and post-translational levels in response to hypoxia and promote adaptation to low O_2.

To date, NDRGs have mostly been studied in cancer cells and far less is known about their normal role and regulation. However, significant insights into their function are likely to result from the recently solved crystal structures of *NDRG1*, *2*, and *3*.[68–70] While all members of this family can be regulated in response to fluctuations in O_2 levels, it is unclear what range and duration of hypoxia they respond to. Lastly, even though the spatial distribution of *NDRG* family members has been analyzed in zebrafish[71,72] and frog (*Xenopus laevis and tropicalis*) embryos[43,73,74] and mammals,[75–83] it is unclear whether their spatial distribution changes under low O_2. We report here on the spatial distribution of members of the zebrafish Ndrg family and their regulation in response to hypoxia.

2 | MATERIALS AND METHODS

2.1 | Zebrafish

Zebrafish (*Danio rerio*) were raised and housed at 27°C on a 14/10 hour light/dark cycle. Zebrafish used in this study were the wild-type AB strain. Embryos were obtained by breeding male/female pairs. Maintenance of zebrafish and experimental procedures on larvae and adult zebrafish were performed in accordance with the protocol approved by the Institutional Animal Care and Use Committee (IACUC) at the University of Maryland Baltimore County. Zebrafish embryos (raised in normoxia) were staged and sorted according to Kimmel et al.[84] See Figure S2 for staging of anoxia-treated embryos.

2.2 | Hypoxia and anoxia treatments

For wholemount in situ hybridization (WISH), 24 hour post-fertilization (24 hpf) zebrafish embryos were dechorionated and then placed in 100 mm petri dish (CellTreat, Pepperell, MA, USA, Cat# 229663) containing 0% or 3% O_2 system water in an O_2 control glove box (Plas-Labs, Lansing, MI, USA model # 856-HYPO) set at 0% or 3% O_2 and 27°C. Following hypoxia treatment, embryos were placed into 1.5 ml microcentrifuge tubes (~20 embryos/tube) with excess water removed. Embryos in each microcentrifuge tube were removed from the chamber and fixed in 4% paraformaldehyde (PFA) in phosphate buffer saline (PBS) (Thermo Scientific, Waltham, MA, USA, Cat# J19943-K2) at 4°C overnight. Fixed embryos were rinsed in absolute methanol (Thermo Fisher Scientific, Waltham, MA, USA, CAS# 67-56-1) for 10 min at room temperature and stored in absolute methanol at −20°C.

For real-time PCR (qPCR), stage-matched control embryos were placed in 100 mm petri dishes containing 0% or 3% O_2 system water, placed in the O_2 control glove box set at 0% or 3% O_2 and 27°C. Following 4 and 8 h of treatment, single embryos were placed into 1.5 ml microcentrifuge tubes (Stellar Scientific Ltd. Co., Albuquerque, NM, USA, Cat# T17-100) with excess water removed. Single embryos in the microcentrifuge tubes were taken out of the chamber, flash frozen in liquid nitrogen, and stored at −80°C for total RNA extraction. Embryos raised under normoxic conditions were used as stage-matched controls for 3% O_2 (27 hpf for 4 h and 30.5 hpf for 8 h) and anoxia (26 hpf for 4 h and 27 hpf for 8 h) treatments.

2.3 | Riboprobe synthesis

The PCR template was cDNA synthesized from total RNA extracted from a combination of 6, 24, and 48 hpf zebrafish embryos. RNA extraction was performed with the QuickRNA MicroPrep Kit (Zymo Research, Irvine, CA, USA, Cat#R1051) and cDNA synthesis was carried out using the iScript cDNA Synthesis Kit (Bio-Rad, Hercules, CA, USA, Cat# 1708890) according to the manufacturers' instructions.

PCR reactions were prepared using 1 μl of diluted (1:5) cDNA as template in a total volume of 50 μl. Primer concentrations were 10 μM for each oligonucleotide. PCR-fragments were produced using a C1000 Thermal Cycler (Bio-Rad, Hercules, CA, USA, Cat#1851148) and Phusion-Polymerase (Thermo Scientific, Vilnius, LT, F530S) (35 cycles and 57°C annealing temperature). PCR-fragments were gel-purified using Micro Bio-Spin P-30 Gel columns Tris Buffer (RNase-free)(Bio-Rad, Hercules, CA, USA, Cat#7326250) and subsequently, 300–500 ng were used as template DNA to synthesize antisense RNA probes using in vitro transcription with the mMESSAGE mMACHINE T7 Transcription Kit (Thermo Fisher Scientific, Carlsbad, CA, USA, Cat#AM1344), incorporating digoxigenin (DIG)-UTP via a DIG-labeling kit (Roche, Mannheim, Germany, Cat#11277073910).

To avoid amplification of regions of homology between *ndrg* members, all oligonucleotide primer pairs were designed against the 3′UTR of each gene, with the exception of *ndrg2* for which the primer pairs targeted the coding region (spanning exons 11-16) as well as the 3′UTR, as

specified in Li et al.[71] For antisense probes, a T7 promoter sequence (5′-TAATACGACTCACTATAG-3′) was added to the 5′ end of each reverse primer. The following primer sets were used to amplify cDNA for 35 cycles as follows:

ndrg1a forward: 5′-ACCAATCAGTTCTGACTGTGCT GC-3′

ndrg1a reverse: 5′-TAATACGACTCACTATAGCACTC CCAACATGGAAAACGCAGA-3′

ndrg1b forward: 5′-ACACGCCTCAGCAGTTTAATCTGG-3′

ndrg1b reverse: 5′-TAATACGACTCACTATAGCTCAC TGAAGTCTTGCACAACCAG-3′

ndrg2 forward: 5′-ACAACACGTTCAAATGCCCG-3′

ndrg2 reverse: 5′-TAATACGACTCACTATAGGGAAGA CATGAGCTGGCTGT-3′

ndrg3a forward: 5′-GGTCTTCCAACTGGTTTGAGATGC-3′

ndrg3a reverse: 5′-TAATACGACTCACTATAGTGAGA ACCAGTGGACAGTGACACT-3′

*ndrg3b*forward:5′-GCCAGAGAGTGCTGGTCTAATGAA-3′

ndrg3b reverse: 5′-TAATACGACTCACTATAGCCGAG ACATGCTAATCAGTAGCTC-3′

ndrg4 forward: 5′-GACTTGCGTCAGGGATGATAACCT-3′

ndrg4 reverse: 5′-TAATACGACTCACTATAGGAATGA GTGAGAGCAAGGGCCGAT-3′

2.4 | Wholemount RNA in situ hybridization

Normoxic controls were fixed at desired stages (shield, 15 somites, 24 hpf, and 48 hpf) in 4% PFA in PBS (Thermo Scientific, Waltham, MA, USA, Cat# J19943-K2) at 4°C overnight. Anoxia-exposed 24 hpf embryos were treated as described in the anoxia treatment section above. To prevent pigmentation from masking the WISH signal, embryos fixed after 24 hpf were incubated in 0.003% 1-phenyl-2-thiourea (PTU) (Sigma-Aldrich, Milwaukee, WI, USA, Cat# P7629-100G) at 24 hpf until the time of fixation. WISH was performed on both normoxic and anoxic embryos using DIG labeled antisense probes according to the specifications published by Thisse and Thisse.[85] Briefly, embryos were rinsed in PBS (137 mM NaCl, 2.7 mM KCl, 8.8 mM Na_2HPO_4) with 0.1% Tween-20 (Sigma-Aldrich, Milwaukee, WI, USA CAS# 9005-64-5). Proteinase K (10 μg/ml; Sigma-Aldrich, Milwaukee, WI, USA CAS# 39450-01-6) treatment was performed for 10 min (24 hpf), 12 min (27 hpf control and 24 hpf + anoxia-treated) and 30 min (48 hpf) embryos. Embryos were then hybridized with DIG labeled antisense probes (in situ hybridization mix with 5% Dextran Sulfate (EMD Millipore Corp., Billerica, MA, USA, Cat#S4030)) at 70°C overnight. Following hybridization, excess probe was removed by washing embryos in a saline-sodium citrate (SSC) series (Thermo Fisher Scientific, Waltham, MA, USA, Cat# AM9763). For probe detection, alkaline phosphatase-conjugated antibody (Roche Diagnostics, Mannheim, Germany, Cat# 11093274910) diluted (1:5,000) in pre-incubation (PI) buffer (PBS, 0.1% Tween 20, 2% sheep serum, 2 mg/ml BSA) (Thermo Fisher Scientific, Waltham, MA, USA, CAS# 9048-46-8) was added and incubated at 4°C overnight. 5-Bromo-4-chloro-3-indolyl-phosphate (BCIP) (Roche, Mannheim, Germany, Cat#11383221001) was used in conjunction with nitro blue tetrazolium (NBT) (Roche, Mannheim, Germany, Cat#11383213001) for the colorimetric detection of alkaline phosphatase activity. When the signal was optimal, the reaction was stopped by washing in PBS with 0.1% Tween-20 and rinsed in 4% PFA overnight.

2.5 | Vibratome sectioning, microscopy, and imaging

Following WISH, embryos were embedded in 4% low melt agarose (IBI Scientific, Peosta, IA, USA, Cat# IB70050) in PBS (100 g/ml) and sectioned using a vibratome (Vibratome, 1500) set at 40 μm thickness. Cross-sections were mounted on glass slides in 50% glycerol (Sigma-Aldrich, Milwaukee, WI, USA, Cat# G7757-1GA) under cover slips.

Zebrafish embryos were mounted for imaging from a lateral or dorsal view on slides, in a drop of 4% w/v methylcellulose (Sigma Aldrich, Milwaukee, WI, USA, Cat# 274437-500G) in 1× E3 medium (5 mM NaCl, 0.17 m 9M KCl, 0.33 mM $CaCl_2$, and 0.33 mM $MgSO_4$) (for zebrafish embryo). Bright-field images were captured using an AxioCam HRc 503 CCD camera mounted on an Axioskop (Carl Zeiss, Oberkochen, Germany). Immunolabeled embryos were imaged on a TCS SP5 confocal microscope (Leica, Wetzlar, Germany). Images were corrected for brightness and contrast along the entire image, and for comparison of normoxia and anoxia treated embryos the images were adjusted equally.

2.6 | Real-time quantitative PCR

RNA extractions and cDNA synthesis were carried out using single embryos collected at the appropriate developmental stage for the stage-matched controls and immediately following treatment for anoxia- and 3% O_2-treated embryos. RNA extractions were performed using the QuickRNA MicroPrep Kit (Zymo Research, Irvine, CA, USA, Cat#R1051). cDNA was synthesized from 100 ng total RNA using iScript cDNA Synthesis Kit (Bio-Rad, Hercules, CA, USA, Cat# 1708890) according to the manufacturers' instructions. The cDNA samples were diluted 1:10 with nuclease-free water (Life Technologies Corp., Austin, TX, USA, Cat# AM9937). qPCR experiments were carried out with a CFX96 Touch Real-time qPCR Detection System (Bio-Rad, Hercules, CA, USA) using the

SsoAdvanced Universal SYBR Green Supermix (Bio-Rad, Hercules, CA, USA, Cat# 172-5271).

We tested a panel of candidate reference genes for the q-PCR analysis, including *ef1a*, *β-actin*, *rpl0*, *rpl13a*, and *ube2a*, which were previously demonstrated to be stable across zebrafish developmental stages and/or following harsh chemical treatments.[27,86–88] Among these, *rpl0*, *rpl13a*, and *ube2a* did not amplify sufficient cDNA in 40 cycles and were not pursued further. *ef1a* and *β-actin* have both been used as reference genes for zebrafish hypoxia studies specifically[27,87] and their transcripts were sufficiently abundant at 24 hpf. We selected *ef1a* for all experiments described below. Oligonucleotide primer pairs spanned regions common to all *ndrg* splice variants, with the exception of *ndrg1b* and *ndrg2*, which only have one variant. The PCR primer efficiency of each primer pair was assessed using cDNA dilution curves and values of 96%–104% were obtained for all except *ndrg1b*, which did not amplify efficiently (consistent with the lack of gene expression at 24 hpf observed using WISH and reported by others[89]). Amplification specificity was determined following each run as the presence of a single melt peak for each transcript. The following primer sets were designed using Primer-BLAST and used to amplify cDNA for 40 cycles:

ndrg1a forward: 5′-ATCATGCAGCACTTCGCTGT-3′
ndrg1a reverse: 5′-CAATAGCCATGCCGATCACA-3′
ndrg1b forward: 5′-CATGGGCTACATGCCCTCTG-3′
ndrg1b reverse: 5′-TGACCCGATGAACTGTGCTC-3′
ndrg2 forward: 5′-AGCTGGAAAGAAAGTGCGAGA-3′
ndrg2 reverse: 5′-TTTACGCCGTCCGCTTATGT-3′
ndrg3a forward: 5′-GGACTAGCAATCTTGTGGAC-3′
ndrg3a reverse: 5′-TCTCGATTCCGAGGTCTTGA-3′
ndrg3b forward: 5′-GTCAGGCTTGATGATGGATG-3′
ndrg3b reverse: 5′-CCCTCTCAAAGTCACATGAAGG-3′
ndrg4 forward: 5′-AGCCAGCTATTCTGACCTAC-3′
ndrg4 reverse: 5′-GATATCCTTGAGGCATCTGG-3′
ef1α forward: 5′-TACCCTCCTCTTGGTCGCTT-3′
ef1α reverse: 5′-TGGAACGGTGTGATTGAGGG-3′

Reactions were run in triplicate with 7–8 biological replicates, using 1 μl of diluted cDNA as template in a reaction volume of 20 μl. For all *ndrg4* reactions, 2 μl of stock cDNA was used as template. Primer stock concentrations were 10 μM and working concentrations were 0.5 μM for each oligonucleotide (Thermo Fisher Scientific, Waltham, MA, USA). The following annealing temperatures were used for each target gene primer set: 57.0°C for *ndrg1a*, 56.6°C for *ndrg2*, 53.0°C for *ndrg3a*, 55.0°C for *ndrg3b*, and 51.0°C for *ndrg4*. Evaluation of results was performed with the CFX96 Touch RT-PCR Detection System program (Bio-Rad, Hercules, CA, USA) and using GraphPad Prism 8 & 9 software (Prism, San Diego, CA, USA). The presence of outliers was assessed using both Grubbs' (alpha = 0.05) and ROUT (Q = 1%) methods. Outliers identified with both Grubbs' (alpha = 0.05) and ROUT (Q = 1%) methods and were further inspected and handled as follows.[90,91] Outliers with Ct values that could not be attributed to experimental error (improper dilution, amplification failure) for a particular group were included, as the variation could be attributed to biological variation. Outliers with Ct values over 40 (e.g., a technical replicate for which amplification did not occur properly) were not further analyzed, and any biological replicates for which two or more technical replicates of the reference or target gene failed to amplify were entirely excluded from the analysis.

2.7 | Immunolabeling

Embryos were fixed in 4% PFA at RT for 1 h and washed in 1× PBS for 30 min on a nutator. Fixed embryos were permeabilized with cooled acetone for 5 min at −20°C, followed by a 5 min wash in 1× PBS. Embryos were subsequently incubated in Inoue blocking solution[92] (5% Normal Goat Serum (NGS)) (Abcam, cat# ab7481, lot# GR325285-5), 2% BSA (Fisher Scientific, cat# BP1600-100, lot# 196941), 1.25% Triton X-100 (Fisher Scientific, cat# BP151-500, lot# 172611) in 1× PBS for 1 h at room temperature (RT) on a rotating platform (80 RPM). Incubation in primary antibodies was performed in I-buffer solution (1% normal goat serum, 2% bovine serum albumin, 1.25 % Triton X-100, in 1× PBS) for 2 days at RT on a rotating platform (80 RPM). Embryos were then washed three times, 30 min each, with 1× PBS at room temperature. Secondary antibodies, diluted in I-buffer, were applied for 1 day at RT on a rotating platform (80 RPM). After secondary antibody incubation, embryos were washed three times with 1× PBS for 30 min.

2.7.1 | Primary antibodies

Anti-NDRG1 (1:200–500) (Sigma Aldrich, catalog # HPA-006881, lot# A69409, rabbit polyclonal).

2.7.2 | Secondary antibodies

Goat anti-rabbit Alexa Fluor 594 (Abcam, cat# ab150080, lot# GR3373513-1).

2.8 | Fluorescence intensity measurements of the pronephric duct

Fluorescence intensity corresponding to Ndrg1a protein levels in the anterior and posterior pronephric duct was

measured using lateral views of immunolabeled embryos. A single tight region of interest (ROI) of the pronephric duct was measured for mean intensity using ImageJ (FIJI) software.

2.9 | Fluorescence intensity measurements of ionocytes

Fluorescence intensity corresponding to Ndrg1a protein levels in ionocytes was measured by drawing a tight ROI around individual ionocytes[10] in the yolk ball and yolk extension using ImageJ (FIJI).

3 | RESULTS

3.1 | The spatial distribution of the *ndrg* family during early development

The zebrafish genome encodes six homologs of the *ndrg* family: *ndrg1a* (ENSDARG00000032849), *ndrg1b* (ENSDARG00000010420), *ndrg2* (ENSDARG00000011170), *ndrg3a* (ENSDARG00000013087), *ndrg3b* (ENSDARG00000010052), and *ndrg4* (ENSDARG00000103937). To characterize the members of the *ndrg* family, we began by determining their spatial distribution in early-stage zebrafish embryos, using WISH. Since several members of this family contain large overlapping coding sequences (53%–65% homology), riboprobes were designed that bind to non-conserved regions in the 3′UTR of all *ndrgs*, with the exception of *ndrg2*. Due to issues with the amplification of the *ndrg2* 3′UTR, we used instead a riboprobe complementary to the coding region and 3′UTR of this gene that has low homology with other *ndrg* members.[71]

At the shield stage (6 hpf), *ndrg1a* expression is ubiquitous (Figure 1A). During segmentation (15-somites), *ndrg1a* becomes restricted to the pronephric ducts (embryonic kidney) and ionocytes (also known as mucous cells; Figure 1B,C); these cell types serve the common function of maintaining osmotic homeostasis by filtering ions across the plasma membrane. *ndrg1a* is also observed in the yolk at this stage of development (Figure 1B). At 24 hpf *ndrg1a* is weakly expressed in the epiphysis (embryonic gland that produces melatonin), in addition to the pronephric duct, ionocytes, and caudal vein (Figure 1D,E) and by 48 hpf, *ndrg1a* is observed in corpuscles of Stannius (endocrine glands in the kidney), liver, intestinal bulb, retina, and other brain regions (Figure 1F,G). The expression of *ndrg1b* is very dynamic. At the shield stage, it is ubiquitously expressed (Figure 1H), while by 15-somites and 24 hpf, it is no longer detected (Figure 1I–L). In contrast, at 48 hpf, *ndrg1b* is strongly expressed in the retina (Figure 1M,N). The expression of *ndrg2* is ubiquitous at shield stage (Figure 2A) and remains broadly distributed by 15-somites, in the embryo proper and the yolk (Figure 2B,C). At 24 hpf, *ndrg2* is strongly expressed in the brain, retina, spinal cord, and intermediate cell mass of the mesoderm (where hematopoiesis occurs; Figure 2D,E). At 48 hpf, *ndrg2* expression expands to the pectoral fin buds, somites and the heart, with basal levels observed throughout the embryo (Figure 2F,G). *ndrg3a* is broadly expressed at the shield stage (Figure 3A) and is observed in the head region and pronephric ducts at 15-somites (Figure 3B,C). At 24 hpf (Figure 3D,E), *ndrg3a* is also seen in pharyngeal pouches, pectoral fin buds and somites. By 48 hpf, *ndrg3a* signal is detected in the brain, cranial placodes, and the spinal cord in addition to the pronephric ducts and associated corpuscles of Stannius (Figure 3F,G). *ndrg3b* signal is not detected between shield stage and 24 hpf (Figure 3H–L); however, at 48 hpf it is observed in the brain and, at lower levels, in pectoral fin buds (Figure 3K,L). At the shield stage, *ndrg4* is expressed ubiquitously (Figure 2H) but becomes enriched in somites by the 15-somites stage (Figure 2I,J). At 24 hpf and 48 hpf (Figure 2K–N), *ndrg4* transcript is detected in the brain, the heart, the cranial placodes, the somites, the spinal cord, the pectoral fin buds, the intermediate cell mass of the mesoderm, and proctodeum.

3.2 | Normoxic control groups that account for hypoxia-induced developmental delays

To gain an understanding of the transcriptional regulation of *ndrgs* in response to low O_2, we exposed 24 hpf embryos to two different hypoxic conditions (3% and 0% O_2) for 4 or 8 h and analyzed transcript levels using qPCR (results presented in section below). Given that O_2 deprivation delays or arrests zebrafish development, an important consideration for these experiments is the appropriate normoxic control group to use, which we have designated as: time zero, age-matched, and staged-matched normoxic controls. Time zero controls are embryos that are the same age as the experimental group at the onset of treatment (i.e., 24 hpf). Age-matched controls are the same age (hpf) as the experimental groups (28 hpf for embryos subjected to 4 h of hypoxia and 32 hpf for embryos exposed to 8 h of hypoxia). Stage-matched controls are embryos at the same developmental stage as the experimental groups exposed to 4 or 8 h of hypoxia; the stage of development varies depending on the severity of the treatment, as embryos arrest faster under anoxia.

With respect to anoxia, when using time zero controls, qPCR results revealed that transcript levels were significantly up-regulated for *ndrg1a* following 4 and 8 h of treatment (3 and 8-fold up-regulation, respectively), while

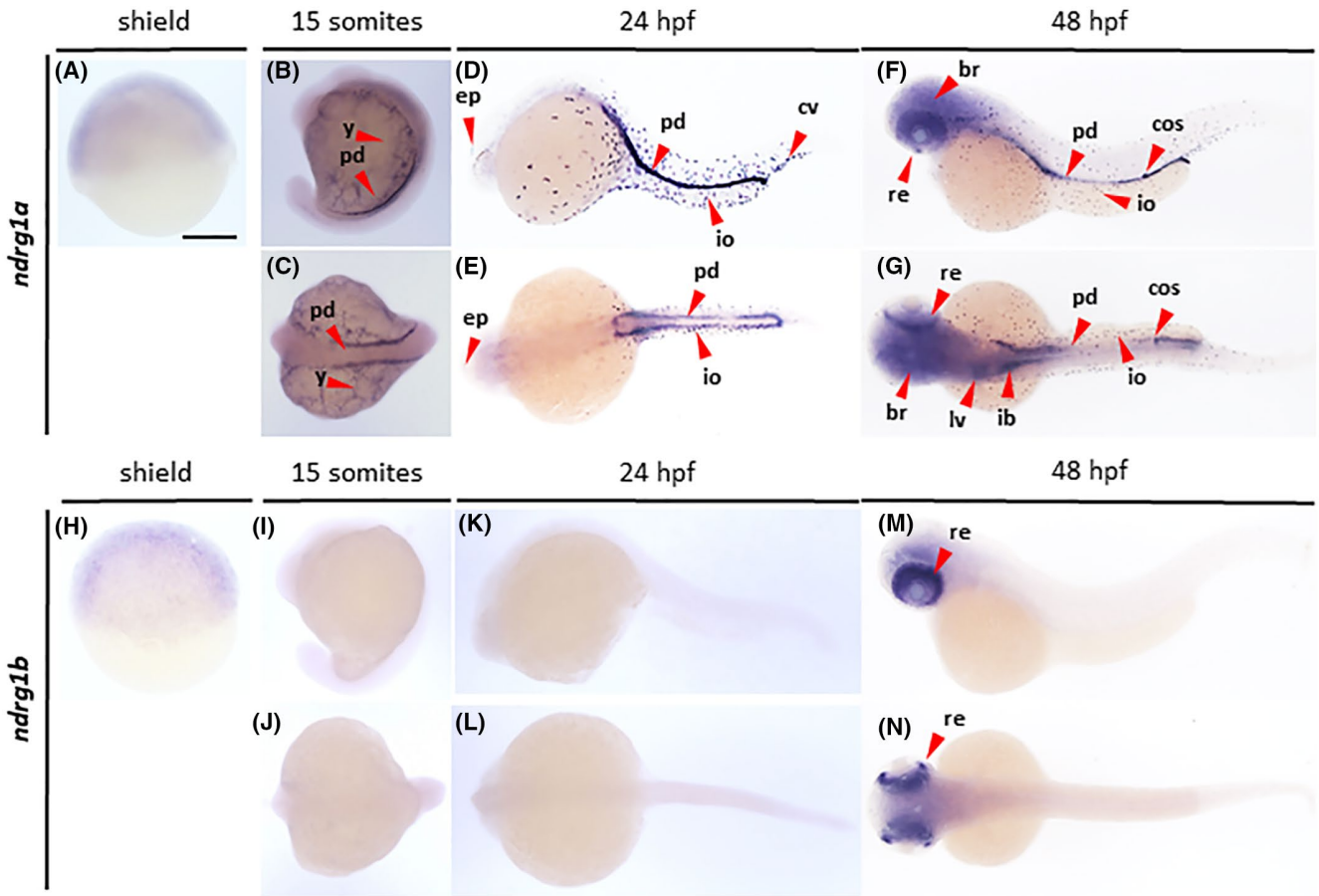

FIGURE 1 Gene expression analysis of *ndrg1*. Wholemount in situ hybridization analysis revealing the distribution of *ndrg1a* (A–G) and *ndrg1b* (H–N) transcripts in zebrafish embryos at shield (A, H), 15 somites (B, C, I, J), 24 hpf (D, E, K, L) and 48 hpf (F, G, M, N) stages, imaged from lateral (A, B, D, F, H, I, K, M) and dorsal (C, E, G, J, L, N) views. br, brain; cos, corpuscles of Stannius; cv, caudal vein; ep, epiphysis; ib, intestinal bulb; io, ionocyte; lv, liver; pd, pronephric ducts; re, retina; y, yolk. Scale bar, 250 μm

other members of the *ndrg* family increased to a lesser extent (2-fold or less; Figure S1A). In contrast, the use of age-matched controls resulted in a different outcome, with *ndrg1a* and *3a* being significantly up-regulated following 4 and 8 h of anoxia while *ndrg2*, *3b* and *4* were down-regulated (Figure S1B). These differences in transcript levels using time zero and age-matched normoxic controls are most likely explained by dynamic gene expression during development, consistent with RNA Seq repository data (EMBL Zebrafish Expression Atlas)[89] showing that *ndrg* expression levels change significantly between 24 and 48 hpf. Based on these observations, the most appropriate normoxic control would be one that takes into account the developmental stage of the experimental group, that is, a stage-matched control.

Several criteria were used to match the developmental stages of experimental groups: the overall length of the embryo, the length of the yolk extension, head curvature, and level of pigmentation of the eye and the body (Figure S2). Based on these criteria, the following normoxic control groups were selected (where = indicates "best matched to"): 26 hpf normoxic control = 24 hpf embryo exposed to 4 h of anoxia (or 24 hpf + 4 h anoxia; Figure S2A,B), 27 hpf normoxic control = 24 hpf + 8 h of anoxia (Figure S2C,D), 27 hpf normoxic control = 24 hpf + 4 h 3% O_2 (Figure S2E,F), 30.5 hpf normoxic control = 24 hpf + 8 h 3% O_2 (Figure S2G,H).

3.3 | Differential regulation of members of the *ndrg* family in response to low oxygen

Cells adapt in distinct manners to varying levels of O_2. Hypoxia (mild to severe) generally elicits metabolic reprogramming via HIF-1α-dependent transcriptional up-regulation of key genes that mediate the adaptive response.[14,15] In contrast, anoxia-tolerance involves metabolic arrest, during which most ATP-demanding processes are suppressed, except for those that are essential for survival.[16,24] To gain an understanding of the range of hypoxia conditions that elicit *ndrg* up-regulation and identify the members of this family that may promote

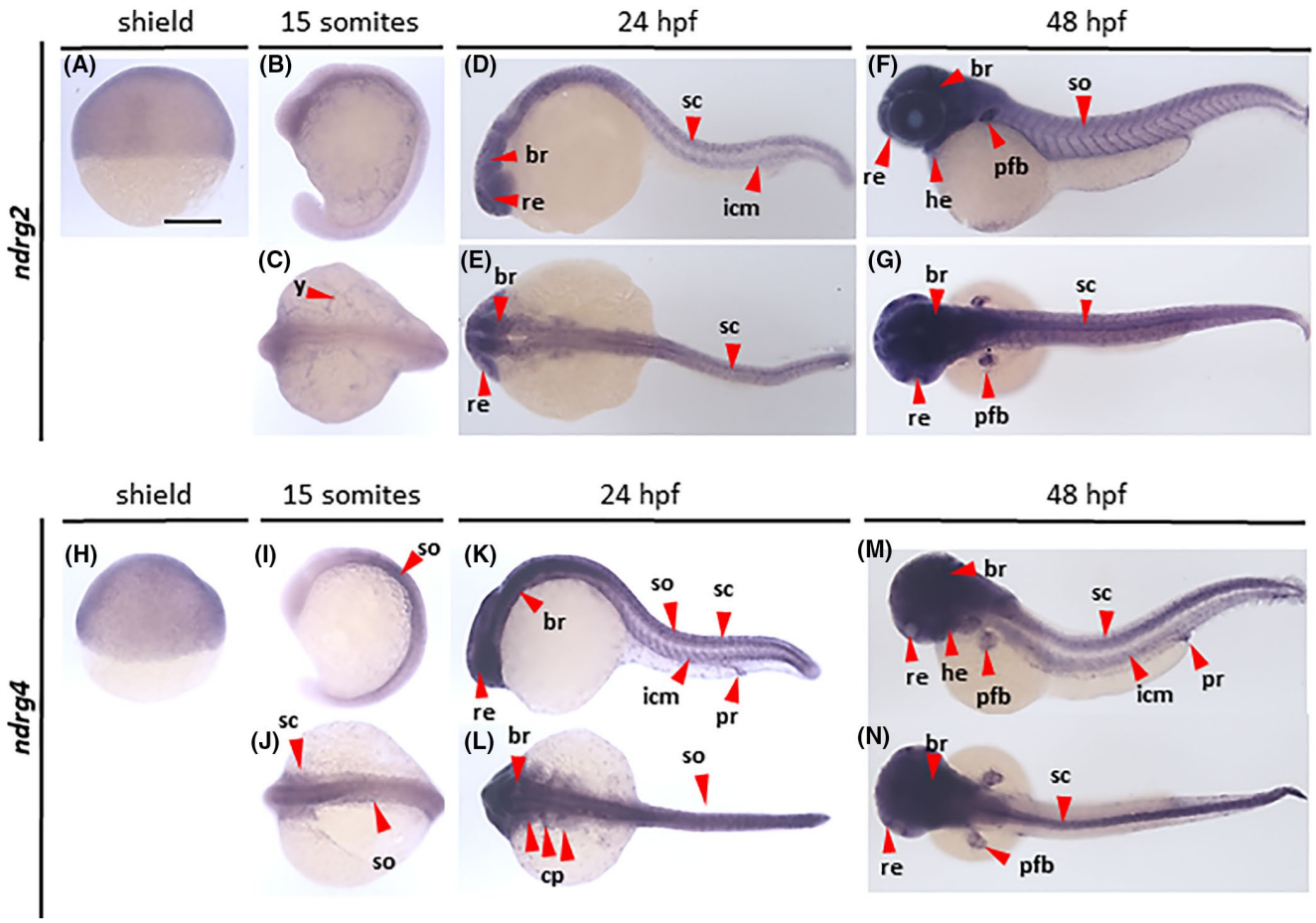

FIGURE 2 Gene expression analysis of *ndrg2* and *ndrg4*. Wholemount in situ hybridization analysis revealing the distribution of *ndrg2* (A–G) and *ndrg4* (H–N) transcripts in zebrafish embryos at shield (A, H), 15 somites (B, C, I, J), 24 hpf (D, E, K, L, J) and 48 hpf (F, G, M, N) stages, imaged from lateral (A, B, D, F, H, I, K, M) and dorsal (C, E, G, J, L, N) views. br, brain; cp, cranial placodes; he, heart; icm, intermediate cell mass of mesoderm; pfb, pectoral fin buds; pr, proctodeum; re, retina; sc, spinal cord; so, somites. Scale bar, 250 μm

hypoxia adaptation, we subjected embryos to hypoxia (3% O_2) or anoxia (0% O_2) for 4 or 8 h.

In response to 4 h of 3% O_2, the transcript levels of none of the *ndrg* family members were significantly altered (Figure 4A). After 8 h of 3% O_2, *ndrg1a* was moderately up-regulated (1.9-fold). The expression of other members was not significantly altered (Figure 4B). These data trends are plotted in Figure 4C.

Following 4 h of anoxia, *ndrg1a* and *ndrg3a* were up-regulated (1.7-fold and 1.5-fold, respectively). In contrast, *ndrg2* was significantly down-regulated (−0.5 fold, respectively), while *ndrg3b* and *ndrg4* expression were not significantly altered (Figure 5A). By 8 h of anoxia, *ndrg1a* was further up-regulated 9.3-fold, and we also observed a slight up-regulation of *ndrg3a* (1.9-fold) (Figure 5B). *ndrg2* was down-regulated (−0.5-fold), and *ndrgb3b* and *ndrg4* did not significantly change following 8 h of anoxia (Figure 5B). These data trends are plotted in Figure 5C.

Overall, these data reveal that the *ndrg* family is differentially regulated in response to low O_2. *ndrg1a* is the most hypoxia-responsive member of the family during early development and is transcriptionally up-regulated in response to severe and prolonged O_2 deprivation. This finding is consistent with a previous study using cancer cells revealing that members of the NDRG family mediate long-term adaptation to hypoxia.[67] Despite the lack of reported HIF-1α binding sites in its promoter region, *ndrg3a* transcript levels also appear to be up-regulated under anoxia. *ndrg1b* levels were extremely low at the stages used in this qPCR analysis (Figure 1K,L) and were not further analyzed. Other members of the *ndrg* family may not be hypoxia-responsive at 24 hpf, at least not at the transcriptional level.

3.4 | The spatial distribution of *ndrg1a* changes in response to anoxia

To confirm that *ndrg1a* is indeed hypoxia-responsive and determine if any changes in its spatial distribution occur following the most stringent hypoxia treatment, we performed WISH using 24 hpf embryos that were exposed

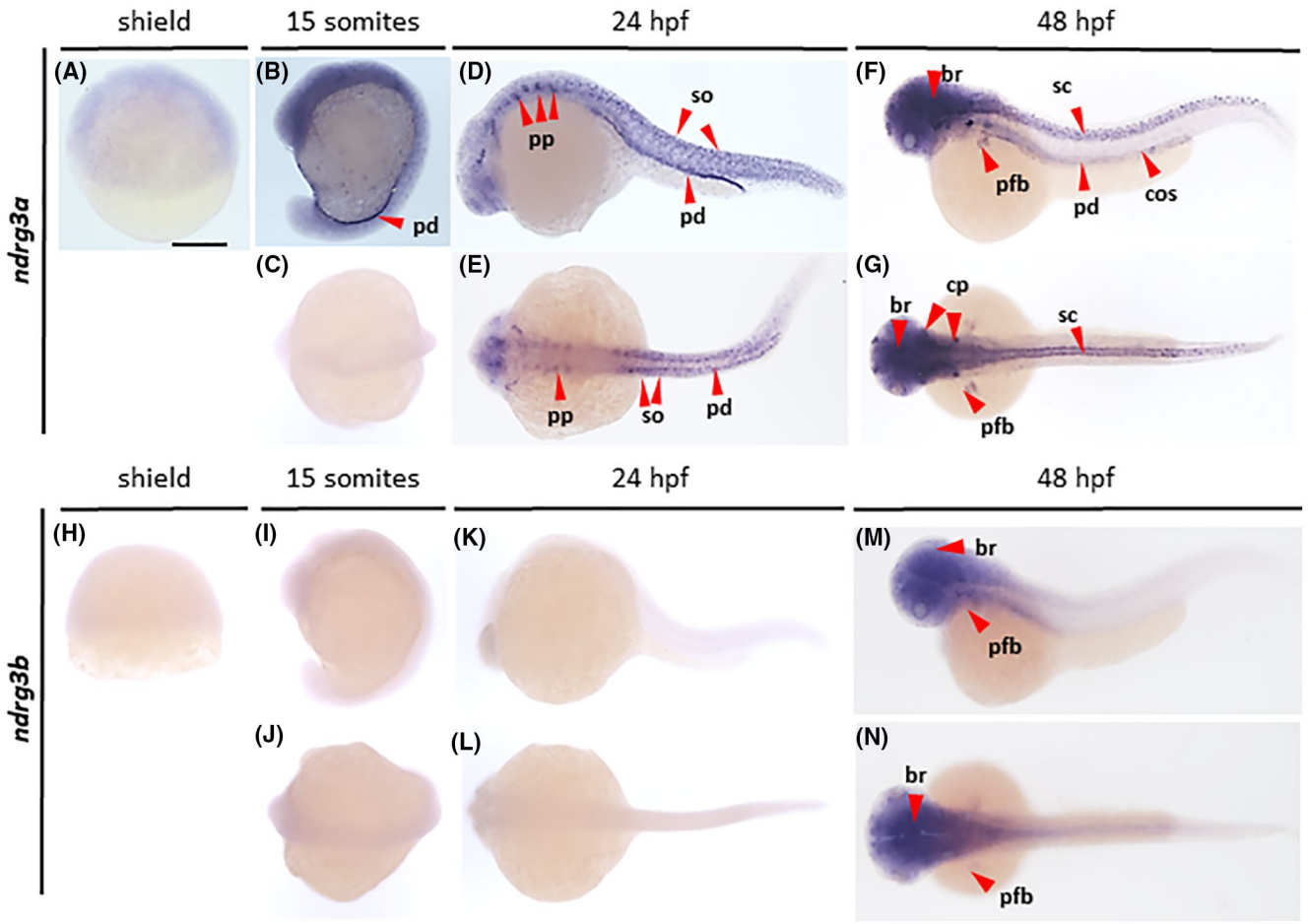

FIGURE 3 Gene expression analysis of *ndrg3*. Wholemount in situ hybridization analysis revealing the distribution of *ndrg3a* (A–G) and *ndrg3b* (H–N) transcripts in zebrafish embryos at shield (A, H), 15 somites (B, C, I, J), 24 hpf (D, E, K, L) and 48 hpf (F, G, M, N) stages, imaged from lateral (A, B, D, F, H, I, K, M) and dorsal (C, E, G, J, L, N) views. br, brain; cos, corpuscles of Stannius; cp, cranial placodes; pfb, pectoral fin buds; pp, pharyngeal pouches; pd, pronephric ducts; sc, spinal cord; so, somites. Scale bar, 250 μm

to 8 h of anoxia. Even though WISH is not a quantitative method to assess gene expression levels, we reasoned that the amount of transcript can at least be directly compared if control (stage-matched) and experimental (anoxia-treated) embryos are processed simultaneously during the color reaction step of WISH.

Following prolonged anoxia, *ndrg1a* transcript was mantained, possibly enhanced, in the pronephric duct, ionocytes, endodermal organs (liver, intestine) and epiphysis (Figure 6B,B′,B″,C,D,F,F″). Interestingly, *ndrg1a* signal was also observed in tissues where this gene is not normally expressed (or expressed at levels that are below the detection limit) under normoxic conditions. Among these tissues, *ndrg1a* was prominently expressed in the inner ear (otic vesicle) (Figure 6B,B′,C,D,F,F′). In addition, *ndrg1a* was observed in the head vasculature in anoxia-treated embryos, namely: the primordial midbrain channel (pmbc), the dorsal aorta (da), the mid-cerebral vein (mcev), and the aortic arch (aa) (Figure 6B,B′,F,F′). Although variable in levels between embryos and experiments (possibly correlating with the duration of the color reaction), *ndrg1a* transcript was also seen in a segmentally-repeated pattern in the trunk (Figure 6A″,B″,C′,D′,E″,F″) that may correspond to somites. The mesoderm-expanded expression explains the thickened anterior-posteriorly oriented stripes of *ndrg1a* label observed from a dorsal view (Figure 6E,F). Furthermore, in samples where the labeling was generally stronger, *ndrg1a* transcript also became apparent in the hatching gland and lateral line primordium, a migrating epithelial placode that deposits a series of mechanosensory hair cell organ progenitors along the flank of the embryo (Figure 6C′). These observations were categorized into mild (Figure 6C-C′), moderate (Figure 6B–B″,F–F″,H, J), and severe (Figure 6D-D′) transcriptional response patterns.

Cross-sections of control and anoxia-treated embryos confirmed the anoxia-induced expression of *ndrg1a* in otic vesicles (Figure 6G,H) and at basal levels throughout the somites, with some puncta of more intense label

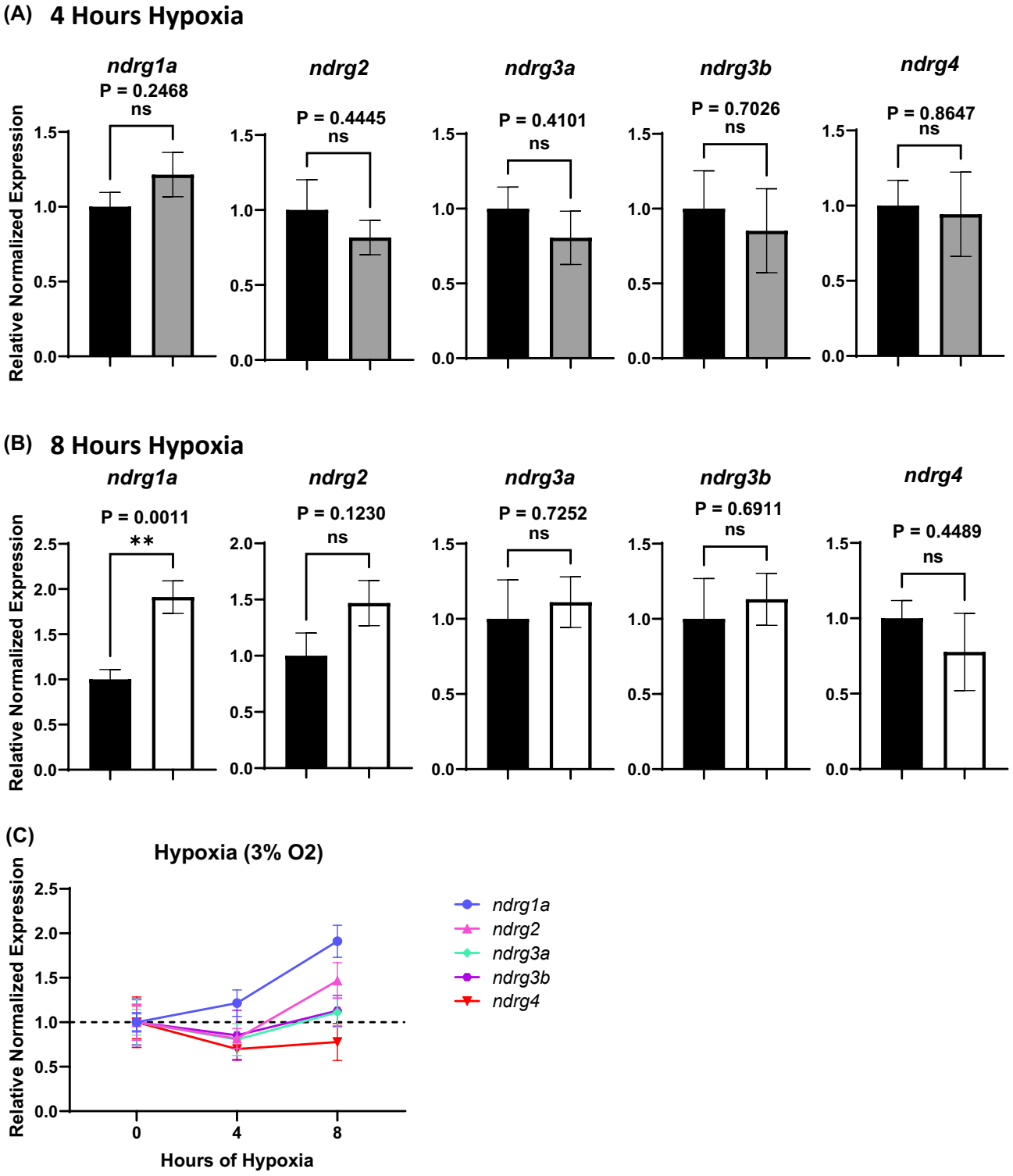

FIGURE 4 Changes in *ndrg* transcript levels in response to hypoxia (3% oxygen). (A, B) Real-time qPCR analysis of 24 hpf zebrafish embryos exposed to 4 h (A, grey bars) or 8 h (B, white bars) of hypoxia relative to normoxic (stage-matched) controls (A, B, black bars) normalized to *ef1a*. (C) Plotted graphical summary of qPCR results. The *y*-axis in the graphs represents the relative normalized expression of each gene. All fold changes were derived using the formula, $2^{-(\Delta\Delta CT)}$, error bars represent standard error of the mean. Significance was obtained using the unpaired, two-tailed *t*-test with Welch's Correction. $^{**}p < .01$. Reactions were run in triplicate with 7–8 biological replicates ($n = 7–8$).

(Figure 6I,J). In addition, the sections revealed elevated expression of *ndrg1a* in the caudal aorta and vein (Figure 6I,J).

To determine whether these changes in *ndrg1a* mRNA expression are also observed at the protein level, we performed immunolabeling using anti-human NDRG1. The

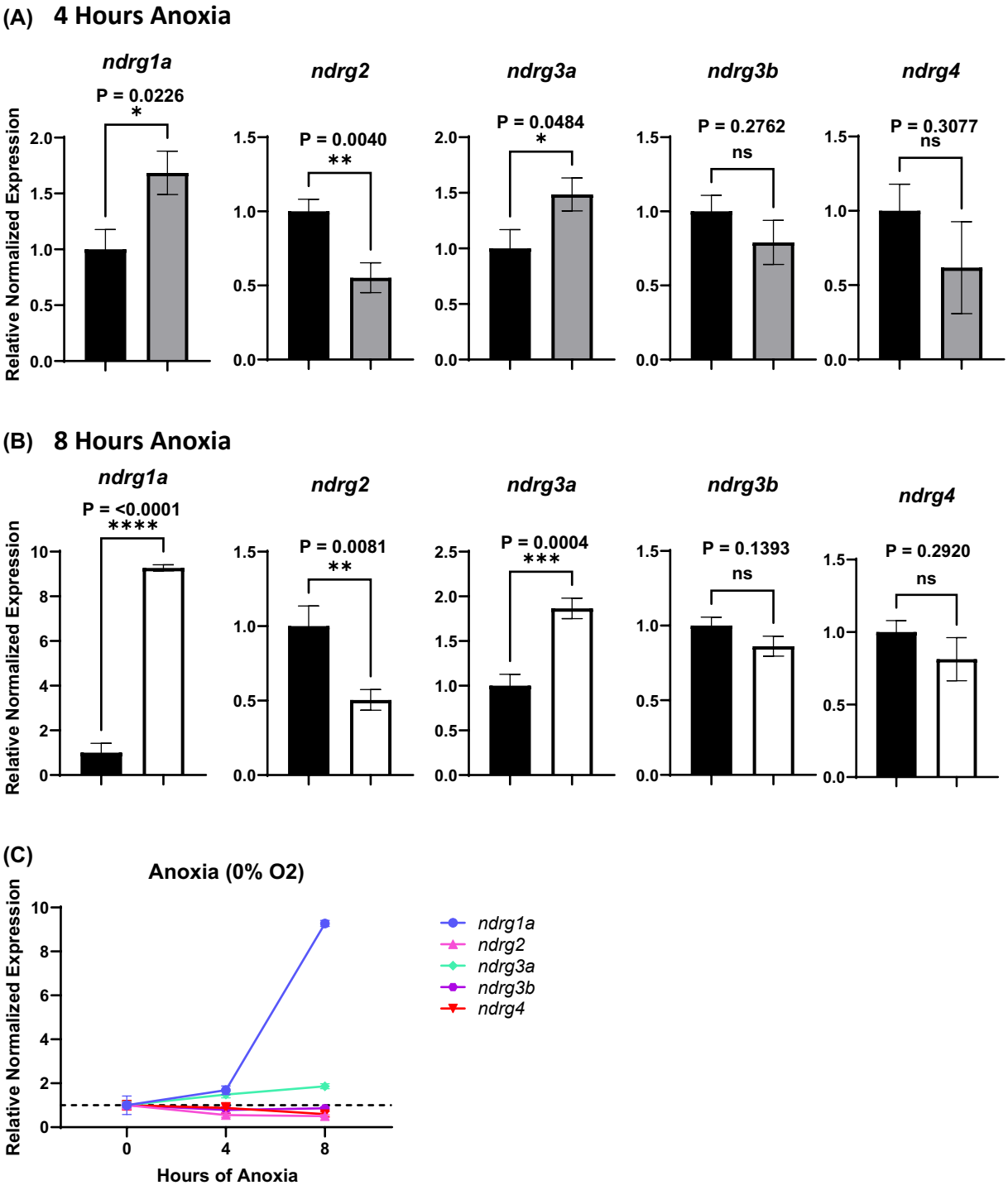

FIGURE 5 Changes in *ndrg* transcript levels in response to anoxia. Real-time qPCR analysis of 24 hpf zebrafish embryos exposed to 4 h (A, grey bars) or 8 h (B, white bars) of anoxia relative to normoxic (stage-matched) controls (A, B, black bars) normalized to *ef1a*. (C) Plotted graphical summary of qPCR results. The *y*-axis in the graphs represents the relative normalized expression of each gene. All fold changes were derived using the formula, $2^{-(\Delta\Delta CT)}$, error bars represent standard error of the mean. Significance was obtained using the unpaired, two-tailed *t*-test with Welch's Correction. *$p < .05$, **$p < .01$, ***$p < .0005$, ****$p < .0001$. Reactions were run in triplicate with 7–8 biological replicates ($n = 7$–8)

duration of anoxia was extended beyond 8 h to include 12 h of treatment ± a period of reoxygenation post-anoxia, anticipating that the mRNA transcribed *de novo* may not be translated immediately or at all under anoxia. Following 8 and 12 h of anoxia (no reoxygenation), Ndrg1a protein level was not noticeably elevated in the pronephric duct

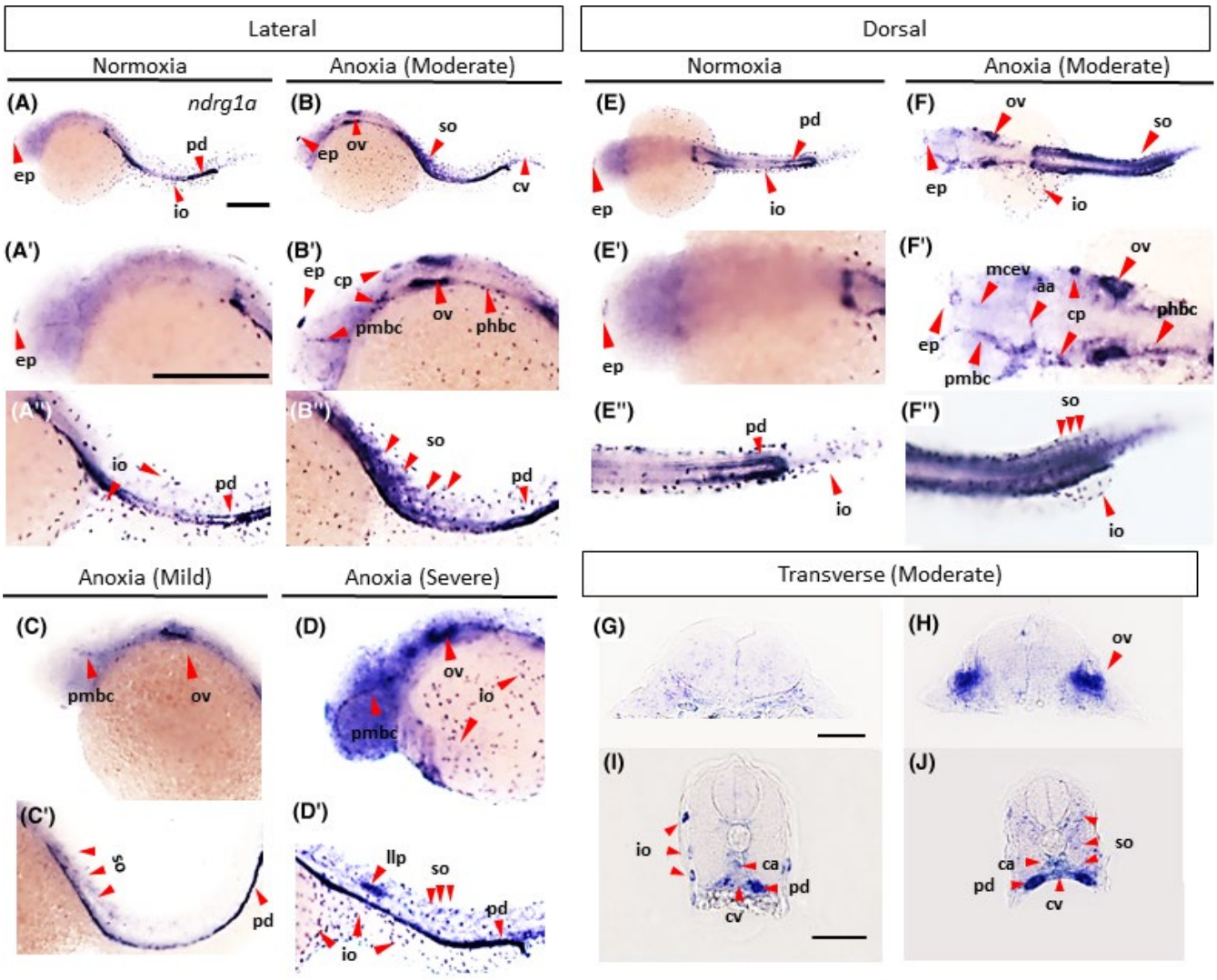

FIGURE 6 Analysis of *ndrg1a* expression in zebrafish embryos following 8 h of anoxia. Wholemount in situ hybridization analysis revealing the distribution of *ndrg1a* transcript in 24 hpf zebrafish embryo exposed to 8 h of anoxia (B–B″, C–C′, D–D′, F–F″, H, J) relative to normoxic (stage-matched controls) (A–A″, E–E″, G, I) imaged from a lateral view (A–D′), a dorsal view (E–F″) and cross-sectional (G–J) views through the otic vesicles (G,H) and the trunk (I,J). (A′–B″, E–F″ are magnified views of (A,B,E,F). The mild (C,C′) and severe (D,D′) transcriptional responses are included to compare with the moderate response (B–B″, F–F″). aa, aortic arch; cp, cranial placodes; cv, caudal vein; da, dorsal aorta; ep, epiphysis; hgc, hatching gland cells; io, ionocyte; llp, lateral line primordium; mcev, mid-cerebral vein; ov, otic vesicle; pcv, posterior cardinal vein; pmbc, primordial midbrain channel; pd, pronephric ducts; so, somites. The experiment was repeated in triplicate, with eight embryos representative of the group imaged. Scale bar in A,A′, 250 μm. Scale bar in G,I, 50 μm

or ionocytes relative to stage-matched normoxic controls (Figure S3A–C′,E), although quantification of fluorescence intensity revealed a slight increase in ionocytes (Figure S3C,F). Furthermore, with the exception of the otic vesicle, in which a weak signal was detected (Figure S3B′,C′), we did not observe Ndrg1a protein in the tissues in which *ndrg1a* transcript increased under anoxia. Interestingly, the addition of 3 h of reoxygenation post-anoxia (12 h) resulted in a striking increase in Ndrg1a protein in the hatching gland, and, to a lesser extent, throughout the head region, the pineal gland, the otic vesicle and the vasculature (posterior cardinal vein and dorsal aorta).

In summary, this analysis revealed that, following prolonged anoxia, *ndrg1a* transcript is maintained or enhanced in tissues in which it is present under normoxic conditions (pronephric duct, ionocytes, and epiphysis) and expanded to additional tissues (vasculature, otic vesicles, and somites). The overall increase in *ndrg1a* across multiple tissues accounts for the dramatic 9-fold up-regulation in transcript observed using qPCR (Figure 5B).

This increase in transcript levels was confirmed at the protein level in some tissues (the hatching gland most prominently), but only following a period of reoxygenation. These findings reveal hypoxia-dependent transcriptional regulation of *ndrg1a* in an intact, developing organism and identify tissues in which *ndrg1a* and other members of this family may play a protective role following hypoxia or upon return to normoxic conditions.

4 | DISCUSSION

4.1 | Expression of *ndrg* family members during early development

WISH analysis of the *ndrg* family shows that during early development (shield), *ndrgs* are broadly expressed, with the exception of *ndrg3b* that is below detection levels (shield to 24 hpf). The overlapping expression of *ndrg1a*, *1b*, *2*, *3a*, *and 4* suggests that these genes may be functionally redundant. From mid-somitogenesis onward, *ndrgs* acquire more distinct spatial distribution patterns, consistent with previous studies revealing expression of members of this family in different cell types in the mouse brain[75] and organs/tissues of *Xenopus laevis* and *tropicalis* embryos.[43,73,74]

The distribution of *ndrgs* is quite similar in fish and amphibian (*Xenopus tropicalis*) embryos. *ndrg1a* is observed in the eye, pronephric duct, intestinal bulb, and liver of zebrafish and *Xenopus* embryos.[43,73,74] However, *ndrg1a* distribution in *Xenopus* appears broader than that of zebrafish, as it is also reported in the frog notochord, branchial arches, and pancreas. Similar to the expression pattern of zebrafish *ndrg2*, the distribution of *Xenopus ndrg2* is enriched in the nervous system; although there are also clear differences between these organisms since zebrafish *ndrg2* is prominent in the heart and somites while *Xenopus ndrg2* is found throughout the epidermis.[43] Zebrafish *ndrg3a* and *Xenopus ndrg3* are both present in cranial placodes and spinal cord, but the former also localizes in the pharyngeal pouches, pronephric duct, and somites while the latter is enriched in the heart and otic vesicles.[43] *ndrg4* is expressed throughout the nervous system in both zebrafish and *Xenopus*, but only observed in the zebrafish intermediate cell mass and proctodeum, and in the *Xenopus* pronephric duct.[43] Overall, these expression patterns suggest that the function of Ndrgs is at least partially conserved between fish and amphibians.

4.2 | *ndrgs* respond differentially to hypoxia

While transcription is an energy-demanding process that is suppressed under severe hypoxia,[17] genes that mediate hypoxia adaptation are generally up-regulated.[14,15] Our qPCR data reveal that among the *ndrg* family members, *ndrg1a* is the most hypoxia-responsive and that prolonged (8 h) anoxia elicits the strongest increase in transcript levels. These findings corroborate with data from previous studies revealing that zebrafish and mammalian NDRG1 have HREs in their promoter region and are up-regulated in a HIF-1α-dependent manner in response to hypoxia.[59,93] *ndrg3*a is also up-regulated under anoxic conditions, albeit to a lesser extent than *ndrg1a* and does not have confirmed HREs, suggesting that other transcription factors contribute to its up-regulation. We observed very high Ct values for *ndrg1b* in our qPCR experiments (data not shown), suggesting low levels of transcript. The low abundance of *ndrg1b* and *ndrg4* at 24 hpf was also reported in an RNA-seq analysis of zebrafish across developmental stages.[89] Our in situ hybridization results for *ndrg1b* also suggest low expression levels around 24 hpf (Figure 1K,L), with expression becoming first noticeable by 48 hpf in the retina. This spatio-temporal expression profile of *ndrg1b* corroborates with previously published data.[94]

Our qPCR data also revealed that *ndrg2*, *3b*, and *4* are either unchanged or down-regulated, which can be explained in several ways. Unchanged values may reflect that the transcripts are stabilized, as previously reported for other genes,[95] or that the rates of synthesis and degradation are equally matched. Down-regulation could be due to mRNA decay exceeding the rate of synthesis or active repression of gene expression to conserve ATP.[16,17,95–97] However, repression seems unlikely, as it is generally reserved for genes whose protein products are required for energetically demanding processes (e.g., *elongation factor 5A* that mediates translation).[17] Given that HREs have been reported in zebrafish *ndrg1a*, *1b* and human *NDRG2* regulatory regions,[58,93] it is surprising that our qPCR analysis revealed that transcript levels of *ndrg2* are either unchanged or decreased under low O_2. It is also possible that a milder hypoxia treatment may be required to elicit up-regulation of *ndrg2*. Surprisingly, we also did not observe significant changes in *ndrg4* transcript levels. Zebrafish *ndrg4* plays essential roles in regulating cardiomyocyte growth and proliferation,[72] processes that should be suppressed under anoxia. *NDRG4* may be regulated by other hypoxia-responsive transcription factors[98] and may also be responsive to milder conditions than those studied here.[99,100] Indeed, a previous study revealed that hypoxia (5%) but not anoxia exposure of 24 hpf zebrafish embryos, caused the up-regulation of *igfbp-1*, *epo*, and *vegf*.[87] Another explanation is that hypoxia-induced transcriptional regulation is dynamic and up-regulation of these genes may occur at later developmental stages, as was previously shown for *igfbp-1 and vegf* that are up-regulated in hypoxia-exposed 36 hpf, but not 24 hpf embryos.[87]

4.3 | *ndrg1a* is up-regulated in metabolically demanding tissues following prolonged anoxia

Previous studies using human cancer cells[59,60] or homogenous cell lines (trophoblasts)[101] have revealed that *NDRG1* is up-regulated in response to hypoxia. However, little is known about how this response is orchestrated across multiple tissues of a whole organism. Using WISH and immunolabeling, we investigated the distribution of Ndrg1a in 24 hpf zebrafish embryos exposed to prolonged anoxia, a treatment that elicits the most robust increase in *ndrg1a* transcript. Given that these conditions are very stringent, we reasoned that any tissue/organ in which Ndrg1a levels are significantly increased must require the activity of this protein to adapt to low O_2.

Our study revealed that, following anoxia, *ndrg1a* is up-regulated in the epiphysis and possibly the pronephric duct, ionocytes, and endodermal organs (although the WISH procedure was not sensitive enough to detect an increase relative to the already high normoxic levels of *ndrg1a* in these cells). The epiphysis, also known as the pineal gland, receives information about the light-dark cycle from the environment and produces the hormone melatonin in response to this information. Melatonin has multiple cellular functions, including reducing oxidative stress,[102] which is elevated under hypoxia and can cause cell death.[103] In addition to responding to light-dark stimuli, the pineal is also hypoxia-responsive, as stabilized Hif-1α modulates clock gene expression in zebrafish pineal cells.[104,105] Given that *ndrg1a* is a Hif-1α target, it is possible that Ndrg1a is implicated in the regulation of clock genes and melatonin production under low O_2.[106] The liver is quite effective at taking up O_2 and is normally well-supplied by the bloodstream; nevertheless, it is susceptible to hypoxic injury and associated complications.[107] In contrast, the intestine normally experiences wide fluctuations in O_2 throughout the day with some regions becoming hypoxic. Genes that aid in the maintenance of the hypoxic intestine are HIF-1α-regulated, providing a potential explanation for the expression of *ndrg1a* in this tissue.[108,109] The function of *ndrg1a* in the pronephric duct and ionocytes is unclear, but these cells rely on the metabolically demanding sodium-potassium ATPase pump to maintain ionic gradients and hence are likely to be sensitive to O_2 depletion.[110]

In addition to enhanced expression of *ndrg1a* in the epiphysis, we also observed expansion of *ndrg1a* distribution to tissues/organs where it is not present under normoxic conditions (or expressed at low levels), namely the inner ear (otic vesicles), head vasculature, and somites. Previous studies have demonstrated that mutations in *NDRG1* are associated with Charcot-Marie-Tooth disease type 4D (CMT4D),[83] a demyelinating neuropathy that causes hearing loss in humans. Furthermore, hypoxia can cause hearing loss[111–114]; thus it is possible that Ndrg1a protects the inner ear or/and connected auditory nerve fibers from hypoxia-induced damage. Vascular sprouting is a well-documented hypoxic response to maximize O_2 delivery.[115] NDRG1 was previously shown to mediate endothelial cell migration under intermittent hypoxia,[116] raising the question of whether its up-regulation under anoxia serves a similar purpose in head vasculature. Somites give rise to skeletal muscle cells, which experience cellular hypoxia and lactic acidosis during exercise that is further exacerbated by environmental hypoxia.[117] It is possible that Ndrg1a protects muscle cells from acidosis or promotes hypometabolism in these cells. The hatching gland is a transient organ that releases enzymes from cytoplasmic granules that mediate hatching of the embryo from its surrounding chorion. Hypoxia is known to induce precocious hatching in zebrafish in a matrix metalloproteinase 13-dependent manner.[118]

In contrast with *ndrg1a* transcript, protein levels did not increase significantly following prolonged exposure to anoxia. Rather, elevated protein levels were observed post-reoxygenation (in the hatching gland most prominently). It is possible that the discrepancy between RNA and protein expression following prolonged hypoxia is due to lack of recognition of a post-translationally modified form of Ndrg1a in some tissues. Alternatively, the *ndrg1a* transcript that is synthesized under hypoxia may mostly be translated post-reoxygenation, possibly to protect cells from oxidative stress or activate other post-hypoxia adaptive responses.[119]

Even though other members of the *ndrg* family are not transcriptionally up-regulated under anoxia (or at least not as significantly as *ndrg1a*), there is evidence that they can be post-translationally modified in response to hypoxia.[67,120–122] In this regard, it is interesting that *ndrg2*, *3a*, *3b*, and *4* are expressed in the pectoral fin buds, which are known to play a respiratory role in fish.[123,124] Furthermore, these genes are expressed in several metabolically demanding tissues, including the brain, spinal cord, heart, and kidney.

In summary, we have shown that *ndrgs* are distributed across a range of hypoxia-sensitive/responsive tissues and that the levels of *ndrg1a* and *3a* are selectively increased following prolonged exposure to anoxia. Future studies will address whether members of this family promote hypoxia adaptation of the tissues and organs in which they are expressed.

ACKNOWLEDGMENTS

We acknowledge P. Chowdhary and B. Weinstein for their helpful comments on our manuscript. We would also like to acknowledge T. deCarvalho and S. Larson for imaging our samples during the COVID-19 pandemic that

limited access to the Keith Porter Imaging Facility. This project was supported by funding from the Department of Defense (W81XWH-16-1-0466) and the National Institute of Health/NICHD (R21HD089476) to R. Brewster. N. Le was supported by a National Institute of Health /NIGMS MARC U*STAR (T34 HHS 00001) National Research Service Award to UMBC. T. Hufford was supported by CBI (NIGMS/NIH T32 GM066706) and IMSD (NIGMS/NIH T32 GM055036) training grants.

DISCLOSURES

The author declares that there is no conflict of interest that could be perceived as prejudicing the impartiality of the research reported.

AUTHOR CONTRIBUTIONS

N. Le executed the WISH and qPCR experiments and analyzed the data; T. Hufford executed qPCR experiments and validation, plotted and analyzed the qPCR data; J. Park optimized and validated immunolabeling reagents, performed immunolabeling experiments, and analyzed the data; and R. Brewster planned and oversaw the project and analyzed the data; N. Le wrote the first draft of the manuscript, T. Hufford and R. Brewster edited the manuscript.

ORCID

Rachel M. Brewster https://orcid.org/0000-0002-9058-2045

REFERENCES

1. Banasiak KJ, Xia Y, Haddad GG. Mechanisms underlying hypoxia-induced neuronal apoptosis. *Prog Neurobiol*. 2000;62:215-249.
2. Nakajima W, Ishida A, Lange MS, et al. Apoptosis has a prolonged role in the neurodegeneration after hypoxic ischemia in the newborn rat. *J Neurosci*. 2000;20:7994-8004.
3. Hu BR, Liu CL, Ouyang Y, Blomgren K, Siesjö BK. Involvement of caspase-3 in cell death after hypoxia-ischemia declines during brain maturation. *J Cereb Blood Flow Metab*. 2000;20:1294-1300.
4. Guo M-F, Yu J-Z, Ma C-G. Mechanisms related to neuron injury and death in cerebral hypoxic ischaemia. *Folia Neuropathol*. 2011;49:79-87.
5. Vohwinkel CU, Hoegl S, Eltzschig HK. Hypoxia signaling during acute lung injury. *J Appl Physiol*. 2015;119:1157-1163.
6. Cummings KW, Bhalla S. Pulmonary vascular diseases. *Clin Chest Med*. 2015;36:235-248.
7. Tanaka S, Tanaka T, Nangaku M. Hypoxia as a key player in the AKI-to-CKD transition. *Am J Physiol-Renal Physiol*. 2014;307:F1187-F1195.
8. Peers C, Dallas ML, Boycott HE, Scragg JL, Pearson HA, Boyle JP. Hypoxia and neurodegeneration. *Ann N Y Acad Sci*. 2009;1177:169-177.
9. Ferdinand P, Roffe C, Hypoxia after stroke: a review of experimental and clinical evidence. *Exp Transl Stroke Med*. 2016;8:1-8.
10. Eltzschig HK, Eckle T. Ischemia and reperfusion—from mechanism to translation. *Nat Med*. 2011;17:1391-1401.
11. Malek M, Nematbakhsh M. Renal ischemia/reperfusion injury; from pathophysiology to treatment. *J Renal Inj Prev*. 2015;4:20-27.
12. Cadenas S. ROS and redox signaling in myocardial ischemia-reperfusion injury and cardioprotection. *Free Radic Biol Med*. 2018;117:76-89.
13. Granger DN, Kvietys PR. Reperfusion injury and reactive oxygen species: the evolution of a concept. *Redox Biol*. 2015;6:524-551.
14. Semenza GL. HIF-1 mediates metabolic responses to intratumoral hypoxia and oncogenic mutations. *J Clin Invest*. 2013;123:3664-3671.
15. Xie H, Simon MC. Oxygen availability and metabolic reprogramming in cancer. *J Biol Chem*. 2017;292:16825-16832.
16. Storey KB, Storey JM. Tribute to P. L. Lutz: putting life on "pause"–molecular regulation of hypometabolism. *J Exp Biol*. 2007;210:1700-1714.
17. Cavadas MAS, Cheong A, Taylor CT. The regulation of transcriptional repression in hypoxia. *Exp Cell Res*. 2017;356: 173-181.
18. Van Den Beucken T, Magagnin MG, Jutten B, et al. Translational control is a major contributor to hypoxia induced gene expression. *Radiother Oncol*. 2011;99:379-384.
19. Wouters BG, Van Den Beucken T, Magagnin MG, Koritzinsky M, Fels D, Koumenis C. Control of the hypoxic response through regulation of mRNA translation. *Semin Cell Dev Biol*. 2005;16:487-501.
20. Koritzinsky M, Seigneuric R, Magagnin MG, Beucken TVD, Lambin P, Wouters BG. The hypoxic proteome is influenced by gene-specific changes in mRNA translation. *Radiother Oncol*. 2005;76:177-186.
21. Ortmann B, Druker J, Rocha S. Cell cycle progression in response to oxygen levels. *Cell Mol Life Sci*. 2014;71:3569-3582.
22. Lees GJ. Inhibition of sodium-potassium-ATPase: a potentially ubiquitous mechanism contributing to central nervous system neuropathology. *Brain Res Rev*. 1991;16:283-300.
23. Helenius IT, Dada LA, Sznajder JI. Role of ubiquitination in Na, K-ATPase regulation during lung injury. *Proc Am Thorac Soc*. 2010;7:65-70.
24. Larson J, Drew KL, Folkow LP, Milton SL, Park TJ. No oxygen? No problem! Intrinsic brain tolerance to hypoxia in vertebrates. *J Exp Biol*. 2014;217:1024-1039.
25. Padilla PA, Roth MB. Oxygen deprivation causes suspended animation in the zebrafish embryo. *Proc Natl Acad Sci*. 2001;98:7331-7335.
26. Mendelsohn BA, Kassebaum BL, Gitlin JD. The zebrafish embryo as a dynamic model of anoxia tolerance. *Dev Dyn*. 2008;237:1780-1788.
27. Ton C, Stamatiou D, Liew CC. Gene expression profile of zebrafish exposed to hypoxia during development. *Physiol Genomics*. 2003;13:97-106.
28. Woods IG, Imam FB. Transcriptome analysis of severe hypoxic stress during development in zebrafish. *Genom Data*. 2015;6:83-88.
29. Julian CG. Epigenomics and human adaptation to high altitude. *J Appl Physiol (1985)*. 2017;123:1362-1370.
30. Storey KB. Anoxia tolerance in turtles: metabolic regulation and gene expression. *Comp Biochem Physiol A Mol Integr Physiol*. 2007;147:263-276.

31. Semenza GL. HIF-1 and mechanisms of hypoxia sensing. *Curr Opin Cell Biol*. 2001;13:167-171.
32. Nakayama K, Kataoka N. Regulation of gene expression under hypoxic conditions. *Int J Mol Sci*. 2019;20:3278.
33. Dengler VL, Galbraith MD, Espinosa JM. Transcriptional regulation by hypoxia inducible factors. *Crit Rev Biochem Mol Biol*. 2014;49:1-15.
34. Schödel J, Mole DR, Ratcliffe PJ. Pan-genomic binding of hypoxia-inducible transcription factors. *Biol Chem*. 2013;394:507-517.
35. Mole DR, Blancher C, Copley RR, et al. Genome-wide association of hypoxia-inducible factor (HIF)-1α and HIF-2α DNA binding with expression profiling of hypoxia-inducible transcripts. *J Biol Chem*. 2009;284:16767-16775.
36. Xia X, Kung AL. Preferential binding of HIF-1 to transcriptionally active loci determines cell-type specific response to hypoxia. *Genome Biol*. 2009;10:R113.
37. Schödel J, Oikonomopoulos S, Ragoussis J, Pugh CW, Ratcliffe PJ, Mole DR. High-resolution genome-wide mapping of HIF-binding sites by ChIP-seq. *Blood*. 2011;117:e207-e217.
38. Benita Y, Kikuchi H, Smith AD, Zhang MQ, Chung DC, Xavier RJ. An integrative genomics approach identifies hypoxia inducible factor-1 (HIF-1)-target genes that form the core response to hypoxia. *Nucleic Acids Res*. 2009;37:4587-4602.
39. Semenza GL. Hypoxia-inducible factors: mediators of cancer progression and targets for cancer therapy. *Trends Pharmacol Sci*. 2012;33:207-214.
40. Takeda N, Maemura K, Imai Y, et al. Endothelial PAS domain protein 1 gene promotes angiogenesis through the transactivation of both vascular endothelial growth factor and its receptor, Flt-1. *Circ Res*. 2004;95:146-153.
41. Wenger RH, Stiehl DP, Camenisch G. Integration of oxygen signaling at the consensus HRE. *Science's STKE*. 2005;2005:re12.
42. Chi J-T, Wang Z, Nuyten DSA, et al. Gene expression programs in response to hypoxia: cell type specificity and prognostic significance in human cancers. *PLoS Med*. 2006;3:e47.
43. Zhong C, Zhou YK, Yang SS, et al. Developmental expression of the N-myc downstream regulated gene (Ndrg) family during *Xenopus tropicalis* embryogenesis. *Int J Dev Biol*. 2015;59:511-517.
44. Melotte V, Qu X, Ongenaert M, et al. The N-myc downstream regulated gene (NDRG) family: diverse functions, multiple applications. *FASEB J*. 2010;24:4153-4166.
45. Shaw E, McCue LA, Lawrence CE, Dordick JS. Identification of a novel class in the α/β hydrolase fold superfamily: the N-myc differentiation-related proteins. *Proteins: Struct Funct Genet*. 2002;47:163-168.
46. Wang B, Li J, Ye Z, Li Z, Wu X. N-myc downstream regulated gene 1 acts as a tumor suppressor in ovarian cancer. *Oncol Rep*. 2014;31:2279-2285.
47. Kalaydjieva L, Gresham D, Gooding R, et al. N-myc downstream-regulated gene 1 is mutated in hereditary motor and sensory neuropathy-Lom. *Am J Hum Genet*. 2000;67:47-58.
48. Taketomi Y, Sunaga K, Tanaka S, et al. Impaired mast cell maturation and degranulation and attenuated allergic responses in Ndrg1-deficient mice. *J Immunol*. 2007;178:7042-7053.
49. Kachhap SK, Faith D, Qian DZ, et al. The N-Myc down regulated Gene1 (NDRG1) is a Rab4a effector involved in vesicular recycling of E-cadherin. *PLoS One*. 2007;2:e844.
50. Sun J, Zhang D, Bae DH, et al. Metastasis suppressor, NDRG1, mediates its activity through signaling pathways and molecular motors. *Carcinogenesis*. 2013;34:1943-1954.
51. Mi L, Zhu F, Yang X, et al. The metastatic suppressor NDRG1 inhibits EMT, migration and invasion through interaction and promotion of caveolin-1 ubiquitylation in human colorectal cancer cells. *Oncogene*. 2017;36:4323-4335.
52. Merlot AM, Porter GM, Sahni S, Lim EG, Peres P, Richardson DR. The metastasis suppressor, NDRG1, differentially modulates the endoplasmic reticulum stress response. *Biochim Biophys Acta Mol Basis Dis*. 2019;1865:2094-2110.
53. Kovacevic Z, Richardson DR. The metastasis suppressor, Ndrg-1: a new ally in the fight against cancer. *Carcinogenesis*. 2006;27:2355-2366.
54. Jin R, Liu W, Menezes S, et al. The metastasis suppressor NDRG1 modulates the phosphorylation and nuclear translocation of beta-catenin through mechanisms involving FRAT1 and PAK4. *J Cell Sci*. 2014;127:3116-3130.
55. Tu LC, Yan X, Hood L, Lin B. Proteomics Analysis of the interactome of N-myc downstream regulated gene 1 and its interactions with the androgen response program in prostate cancer cells. *Mol Cell Proteomics*. 2007;6:575-588.
56. Pietiainen V, Vassilev B, Blom T, et al. NDRG1 functions in LDL receptor trafficking by regulating endosomal recycling and degradation. *J Cell Sci*. 2013;126:3961-3971.
57. Askautrud HA, Gjernes E, Gunnes G, et al. Global gene expression analysis reveals a link between NDRG1 and vesicle transport. *PLoS One*. 2014;9:e87268.
58. Wang L, Liu N, Yao L, et al. NDRG2 is a new HIF-1 target gene necessary for hypoxia-induced apoptosis in A549 cells. *Cell Physiol Biochem*. 2008;21:239-250.
59. Wang Q, Li L-H, Gao G-D, et al. HIF-1α up-regulates NDRG1 expression through binding to NDRG1 promoter, leading to proliferation of lung cancer A549 cells. *Mol Biol Rep*. 2013;40:3723-3729.
60. Cangul H. Hypoxia upregulates the expression of the NDRG1 gene leading to its overexpression in various human cancers. *BMC Genet*. 2004;5:27.
61. Cangul H, Salnikow K, Yee H, Zagzag D, Commes T, Costa M. Enhanced overexpression of an HIF-1/hypoxia-related protein in cancer cells. *Environ Health Perspect*. 2002;110(Suppl 5):783-788.
62. Ellen TP, Ke Q, Zhang P, Costa M. NDRG1, a growth and cancer related gene: regulation of gene expression and function in normal and disease states. *Carcinogenesis*. 2008;29:2-8.
63. Said HM, Safari R, Al-Kafaji G, et al. Time- and oxygen-dependent expression and regulation of NDRG1 in human brain cancer cells. *Oncol Rep*. 2017;37:3625-3634.
64. Yeh CC, Luo JL, Nhut Phan N, et al. Different effects of long noncoding RNA NDRG1-OT1 fragments on NDRG1 transcription in breast cancer cells under hypoxia. *RNA Biol*. 2018;15:1487-1498.
65. Lin HC, Yeh CC, Chao LY, et al. The hypoxia-responsive lncRNA NDRG-OT1 promotes NDRG1 degradation via ubiquitin-mediated proteolysis in breast cancer cells. *Oncotarget*. 2018;9:10470-10482.
66. Lee GY, Chun Y-S, Shin H-W, Park J-W. Potential role of the N-MYC downstream-regulated gene family in reprogramming cancer metabolism under hypoxia. *Oncotarget*. 2016;7:57442-57451.

67. Lee DC, Sohn HA, Park ZY, et al. A lactate-induced response to hypoxia. *Cell*. 2015;161:595-609.
68. Mustonen V, Muruganandam G, Loris R, Kursula P, Ruskamo S. Crystal and solution structure of NDRG1, a membrane-binding protein linked to myelination and tumour suppression. *FEBS J*. 2020;288:3507–3529.
69. Hwang J, Kim Y, Kang HB, et al. Crystal structure of the human N-Myc downstream-regulated gene 2 protein provides insight into its role as a tumor suppressor. *J Biol Chem*. 2011;286:12450-12460.
70. Kim KR, Kim KA, Park JS, et al. Structural and biophysical analyses of human N-Myc downstream-regulated gene 3 (NDRG3) protein. *Biomolecules*. 2020;10:90.
71. Li RA, Traver D, Matthes T, Bertrand JY. Ndrg1b and fam49ab modulate the PTEN pathway to control T-cell lymphopoiesis in the zebrafish. *Blood*. 2016;128:3052-3060.
72. Qu X, Jia H, Garrity DM, et al. ndrg4 is required for normal myocyte proliferation during early cardiac development in zebrafish. *Dev Biol*. 2008;317:486-496.
73. Kyuno J, Fukui A, Michiue T, Asashima M. Identification and characterization of Xenopus NDRG1. *Biochem Biophys Res Commun*. 2003;309:52-57.
74. Zhang T, Guo X, Chen Y. Retinoic acid-activated Ndrg1a represses Wnt/beta-catenin signaling to allow Xenopus pancreas, oesophagus, stomach, and duodenum specification. *PLoS One*. 2013;8:e65058.
75. Okuda T, Kokame K, Miyata T. Differential expression patterns of NDRG family proteins in the central nervous system. *J Histochem Cytochem*. 2008;56:175-182.
76. Schonkeren SL, Massen M, van der Horst R, Koch A, Vaes N & Melotte V. Nervous NDRGs: the N-myc downstream–regulated gene family in the central and peripheral nervous system. *Neurogenetics*. 2019;20173-186.
77. Hu XL, Liu XP, Deng YC, et al. Expression analysis of the NDRG2 gene in mouse embryonic and adult tissues. *Cell Tissue Res*. 2006;325:67-76.
78. Mitchelmore C, Büchmann-Møller S, Rask L, West MJ, Troncoso JC, Jensen NA. NDRG2: a novel Alzheimer's disease associated protein. *Neurobiol Dis*. 2004;16:48-58.
79. Jin PP, Xia F, Ma BF, et al. Spatiotemporal expression of NDRG2 in the human fetal brain. *Ann Anat*. 2019;221:148-155.
80. Maeda A, Hongo S, Miyazaki A. Genomic organization, expression, and comparative analysis of noncoding region of the rat Ndrg4 gene. *Gene*. 2004;324:149-158.
81. Nakada N, Hongo S, Ohki T, Maeda A, Takeda M. Molecular characterization of NDRG4/Bdm1 protein isoforms that are differentially regulated during rat brain development. *Brain Res Dev Brain Res*. 2002;135:45-53.
82. Zhou RH, Kokame K, Tsukamoto Y, Yutani C, Kato H, Miyata T. Characterization of the human NDRG gene family: a newly identified member, NDRG4, is specifically expressed in brain and heart. *Genomics*. 2001;73:86-97.
83. Berger P, Sirkowski EE, Scherer SS, Suter U. Expression analysis of the N-Myc downstream-regulated gene 1 indicates that myelinating Schwann cells are the primary disease target in hereditary motor and sensory neuropathy-Lom. *Neurobiol Dis*. 2004;17:290-299.
84. Kimmel CB, Ballard WW, Kimmel SR, Ullmann B, Schilling TF. Stages of embryonic development of the zebrafish. *Dev Dyn*. 1995;203:253-310.
85. Thisse C, Thisse B. High-resolution in situ hybridization to whole-mount zebrafish embryos. *Nat Protoc*. 2008;3:59-69.
86. McCurley AT, Callard GV. Characterization of housekeeping genes in zebrafish: male-female differences and effects of tissue type, developmental stage and chemical treatment. *BMC Mol Biol*. 2008;9:102.
87. Robertson CE, Wright PA, Köblitz L, Bernier NJ. Hypoxia-inducible factor-1 mediates adaptive developmental plasticity of hypoxia tolerance in zebrafish, Danio rerio. *Proc Biol Sci*. 2014:281:1-9.
88. Xu H, Li C, Zeng Q, Agrawal I, Zhu X, Gong Z. Genome-wide identification of suitable zebrafish Danio rerio reference genes for normalization of gene expression data by RT-qPCR. *J Fish Biol*. 2016;88:2095-2110.
89. White RJ, Collins JE, Sealy IM, et al. A high-resolution mRNA expression time course of embryonic development in zebrafish. *eLife*. 2017;6:e30860.
90. Burns MJ, Nixon GJ, Foy CA, Harris N. Standardisation of data from real-time quantitative PCR methods—evaluation of outliers and comparison of calibration curves. *BMC Biotechnol*. 2005;5:31.
91. Motulsky HJ, Brown RE. Detecting outliers when fitting data with nonlinear regression—a new method based on robust nonlinear regression and the false discovery rate. *BMC Bioinformatics*. 2006;7:123.
92. Inoue D, Wittbrodt J. One for all—a highly efficient and versatile method for fluorescent immunostaining in fish embryos. *PLoS One*. 2011;6:e19713.
93. Greenald D, Jeyakani J, Pelster B, Sealy I, Mathavan S, van Eeden FJ. Genome-wide mapping of Hif-1alpha binding sites in zebrafish. *BMC Genomics*. 2015;16:923.
94. Takita S, Wada Y, Kawamura S. Effects of NDRG1 family proteins on photoreceptor outer segment morphology in zebrafish. *Sci Rep*. 2016;6:36590.
95. Teodoro RO, O'Farrell PH. Nitric oxide-induced suspended animation promotes survival during hypoxia. *EMBO J*. 2003;22:580-587.
96. Johnson AB, Denko N, Barton MC. Hypoxia induces a novel signature of chromatin modifications and global repression of transcription. *Mutat Res*. 2008;640:174-179.
97. Cavadas MAS, Mesnieres M, Crifo B, et al. REST is a hypoxia-responsive transcriptional repressor. *Sci Rep*. 2016;6:31355.
98. Cummins EP, Taylor CT. Hypoxia-responsive transcription factors. *Pflugers Arch*. 2005;450:363-371.
99. Wen L, Liu L, Tong L, et al. NDRG4 prevents cerebral ischemia/reperfusion injury by inhibiting neuronal apoptosis. *Genes Dis*. 2019;6:448-454.
100. Xing Y, Tang B, Zhu C, et al. N-myc downstream-regulated gene 4, up-regulated by tumor necrosis factor-α and nuclear factor kappa B, aggravates cardiac ischemia/reperfusion injury by inhibiting reperfusion injury salvage kinase pathway. *Basic Res Cardiol*. 2016;111:11.
101. Chen B, Nelson DM, Sadovsky Y. N-myc down-regulated gene 1 modulates the response of term human trophoblasts to hypoxic injury. *J Biol Chem*. 2006;281:2764-2772.
102. Claustrat B, Leston J. Melatonin: physiological effects in humans. *Neurochirurgie*. 2015;61:77-84.
103. Niizuma K, Endo H, Chan PH. Oxidative stress and mitochondrial dysfunction as determinants of ischemic neuronal death and survival. *J Neurochem*. 2009;109(Suppl 1):133-138.

104. Chilov D, Hofer T, Bauer C, Wenger RH, Gassmann M. Hypoxia affects expression of circadian genes PER1 and CLOCK in mouse brain. *FASEB J*. 2001;15:2613-2622.
105. Pelster B, Egg M. Hypoxia-inducible transcription factors in fish: expression, function and interconnection with the circadian clock. *J Exp Biol*. 2018;221:1-13.
106. Reiter RJ, Mayo JC, Tan DX, Sainz RM, Alatorre-Jimenez M, Qin L. Melatonin as an antioxidant: under promises but over delivers. *J Pineal Res*. 2016;61:253-278.
107. Ebert EC. Hypoxic liver injury. *Mayo Clin Proc*. 2006;81:1232-1236.
108. Zheng L, Kelly CJ, Colgan SP. Physiologic hypoxia and oxygen homeostasis in the healthy intestine. A review in the theme: cellular responses to hypoxia. *Am J Physiol Cell Physiol*. 2015;309:C350-C360.
109. Singhal R, Shah YM. Oxygen battle in the gut: hypoxia and hypoxia-inducible factors in metabolic and inflammatory responses in the intestine. *J Biol Chem*. 2020;295:10493-10505.
110. Bogdanova A, Petrushanko IY, Hernansanz-Agustin P, Martinez-Ruiz A. "Oxygen Sensing" by Na, K-ATPase: these miraculous thiols. *Front Physiol*. 2016;7:314.
111. Mazurek B, Haupt H, Georgiewa P, Klapp BF, Reisshauer A. A model of peripherally developing hearing loss and tinnitus based on the role of hypoxia and ischemia. *Med Hypotheses*. 2006;67:892-899.
112. Olivetto E, Simoni E, Guaran V, Astolfi L, Martini A. Sensorineural hearing loss and ischemic injury: development of animal models to assess vascular and oxidative effects. *Hear Res*. 2015;327:58-68.
113. Sonbay Yilmaz ND, Saka C, Oktay Arslan B, et al. The effect of hypoxia on hearing function. *Turk J Med Sci*. 2019;49:1450-1454.
114. Sanchez-Garcia MA, Zottoli SJ, Roberson LM. Hypoxia has a lasting effect on fast-startle behavior of the tropical fish *Haemulon plumieri*. *Biol Bull*. 2019;237:48-62.
115. Krock BL, Skuli N, Simon MC. Hypoxia-induced angiogenesis: good and evil. *Genes Cancer*. 2011;2:1117-1133.
116. Toffoli S, Delaive E, Dieu M, Feron O, Raes M, Michiels C. NDRG1 and CRK-I/II are regulators of endothelial cell migration under intermittent hypoxia. *Angiogenesis*. 2009;12:339-354.
117. Gladden LB. Lactate metabolism: a new paradigm for the third millennium. *J Physiol*. 2004;558:5-30.
118. Small CD, El-Khoury M, Deslongchamps G, Benfey TJ, Crawford BD. Matrix metalloproteinase 13 activity is required for normal and hypoxia-induced precocious hatching in zebrafish embryos. *J Dev Biol*. 2020;8:3.
119. Orellana-Urzúa S, Rojas I, Líbano L, Rodrigo R. Pathophysiology of ischemic stroke: role of oxidative stress. *Curr Pharm Des*. 2020;26:4246-4260.
120. Sugiki T, Murakami M, Taketomi Y, Kikuchi-Yanoshita R, Kudo I. N-myc downregulated gene 1 is a phosphorylated protein in mast cells. *Biol Pharm Bull*. 2004;27:624-627.
121. Murray JT, Campbell DG, Morrice N, et al. Exploitation of KESTREL to identify NDRG family members as physiological substrates for SGK1 and GSK3. *Biochem J*. 2004;384:477-488.
122. Burchfield JG, Lennard AJ, Narasimhan S, et al. Akt mediates insulin-stimulated phosphorylation of Ndrg2: evidence for cross-talk with protein kinase C theta. *J Biol Chem*. 2004;279:18623-18632.
123. Zimmer AM, Mandic M, Rourke KM, Perry SF. Breathing with fins: do the pectoral fins of larval fishes play a respiratory role? *Am J Physiol Regul Integr Comp Physiol*. 2020;318:R89-R97.
124. Hale ME. Developmental change in the function of movement systems: transition of the pectoral fins between respiratory and locomotor roles in zebrafish. *Integr Comp Biol*. 2014;54:238-249.

SUPPORTING INFORMATION

Additional supporting information may be found in the online version of the article at the publisher's website.

How to cite this article: Le N, Hufford TM, Park JS, Brewster RM. Differential expression and hypoxia-mediated regulation of the N-myc downstream regulated gene family. *FASEB J*. 2021;35:e21961. doi:10.1096/fj.202100443R